Chemical Engineering Communications

ISSN: 0098-6445 (Print) 1563-5201 (Online) Journal homepage: www.tandfonline.com/journals/gcec20

Carbon nanotubes (CNTs) and graphene oxide (GO) hybrid enhanced canola protein isolate (CPI) bioadhesive for interior wood applications

Michael Enemuo, Ashiegbu Darlington & Olumide Ogunmodimu

To cite this article: Michael Enemuo, Ashiegbu Darlington & Olumide Ogunmodimu (2025) Carbon nanotubes (CNTs) and graphene oxide (GO) hybrid enhanced canola protein isolate (CPI) bioadhesive for interior wood applications, Chemical Engineering Communications, 212:6, 950-967, DOI: 10.1080/00986445.2024.2445226

To link to this article: https://doi.org/10.1080/00986445.2024.2445226

Published online: 27 Dec 2024.

CHEMICAL ENGINEERING COMMUNICATIONS
2025, VOL. 212, NO. 6, 950–967
https://doi.org/10.1080/00986445.2024.2445226

Taylor & Francis
Taylor & Francis Group

Carbon nanotubes (CNTs) and graphene oxide (GO) hybrid enhanced canola protein isolate (CPI) bioadhesive for interior wood applications

Michael Enemuo[a,b], Ashiegbu Darlington[a], and Olumide Ogunmodimu[b]

[a]School of Chemical and Metallurgical Engineering, University of the Witwatersrand, Johannesburg, South Africa; [b]Department of Energy and Mineral Engineering (EME), The Pennsylvania State University, University Park, Pennsylvania, USA

ABSTRACT

Growing concerns over the use of carcinogenic formaldehyde-based wood adhesives drive the need for sustainable alternatives. This study explores a novel nanocomposite adhesive made from canola protein isolate (CPI), reinforced with carbon nanotubes (CNTs) and graphene oxide (GO), to enhance bio-based adhesive performance. CNTs contribute mechanical strength, electrical conductivity, and thermal stability, while GO provides a large surface area, good dispersibility, and enhanced adhesion. The synergistic interaction between these nanomaterials significantly improves the adhesive properties of CPI. The study examined the impact of varying CNT-GO ratios on CPI's adhesive strength under dry, wet, and soaked conditions. Results showed a positive correlation between increasing CNT-GO concentrations and adhesive performance. The adhesive strength markedly increased at a 0.5/0.5 (CNT/GO) ratio, especially in dry conditions. The optimal shear strength, however, was observed at a 0.3/0.7 ratio across all conditions. The thermogravimetric analysis confirmed that higher CNT-GO ratios enhanced the thermal stability of the nanocomposite, as indicated by increased weight loss percentages. This reflects improved resistance of the CPI matrix to thermal degradation. These findings highlight the importance of optimizing CNT-GO ratios for superior performance under diverse conditions. Overall, this study demonstrates the potential of CPI-CNT-GO nanocomposites as more sustainable alternatives to traditional formaldehyde-based adhesives, offering a promising solution to reduce the environmental and health risks associated with conventional wood adhesives.

KEYWORDS

Bioadhesive; canola protein isolate; carbon nanotubes; graphene oxide; nanocomposite; Protein adhesives; wood adhesives

GRAPHICAL ABSTRACT

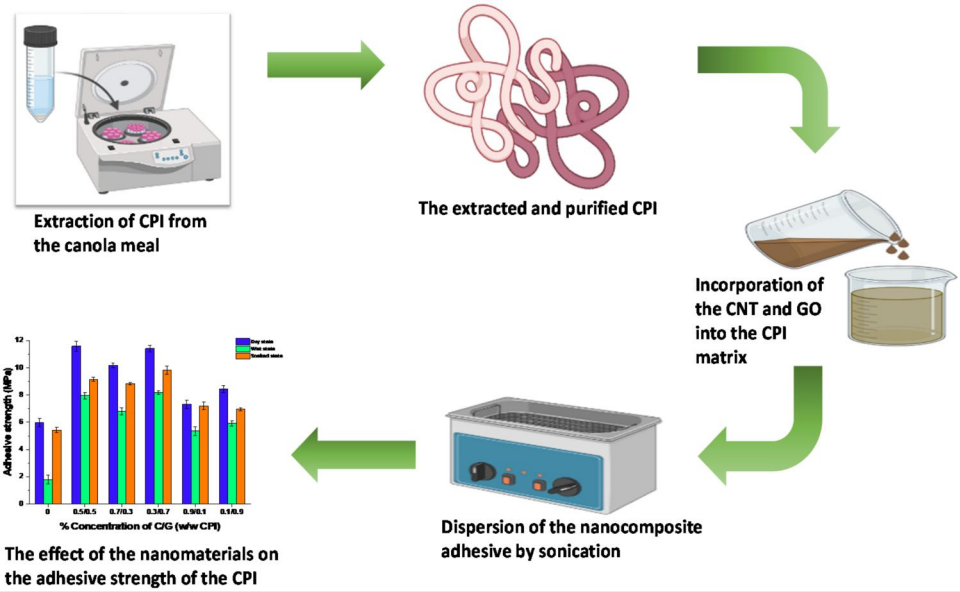

CONTACT Michael Enemuo emichael.enemuo@gmail.com School of Chemical and Metallurgical Engineering, University of the Witwatersrand, 1 Jorissen St, Johannesburg 2017, South Africa.

Introduction

The urgency for sustainable and innovative solutions to confront multifaceted challenges has become increasingly evident in today's dynamic global landscape. Within this context, nanomaterials have emerged as a promising frontier for creating advanced materials endowed with superior properties. Nanomaterials, such as CNT and GO, have garnered significant attention due to their remarkable mechanical, thermal, and electrical properties. Moreover, these nanomaterials also demonstrate a readiness to transfer these properties into new materials (Kong 2013; Khan et al. 2016; Kausar et al. 2017; Bakhtiari et al. 2020; Liu et al. 2020).

Conventional wood adhesives, predominantly formulated with formaldehyde, give rise to significant environmental and health concerns due to the carcinogenic classification of formaldehyde emissions associated with these adhesives (Solt et al. 2019; Gonçalves et al. 2021; Chrobak et al. 2022). Formaldehyde, known for its potential to induce eye, nose, and throat irritation, manifests symptoms including coughing, wheezing, and shortness of breath. Moreover, prolonged exposure to formaldehyde raises concerns about its potential contribution to the development of chronic respiratory diseases, affecting lung function over an extended period (Dan et al. 2020; Dugheri et al. 2021; J. Lam et al. 2021; Wartew 1983). Numerous countries and regions have instituted emission standards targeting formaldehyde emanating from wood products and adhesives to address these risks (Salem and Böhm 2013; Istek et al. 2018; Zhang et al. 2018; Salthammer 2019). These regulatory standards curtail formaldehyde emissions, mitigating the associated health risks.

In response to these challenges, this research embarks on synthesizing novel nanocomposite bioadhesives, including a strategic blend of CNT, GO, and CPI. Recently, CPI has emerged as a promising bio-based adhesive for wood applications due to its biodegradability and renewable origin. Its preparation typically involves defatting canola meal followed by protein extraction through alkali solubilization and isoelectric precipitation, as demonstrated by several studies (Li et al. 2017; Bandara et al. 2018). These articles highlight that although CPI exhibits good adhesion properties, it still faces challenges such as high viscosity and limited water resistance. Researchers have explored modifications and nanomaterial reinforcement strategies to address these drawbacks, thus broadening CPI's application scope as a viable alternative to traditional formaldehyde-based adhesives While CPI exhibits commendable wood bonding performance, it also faces drawbacks such as high viscosity and relatively low water resistance (Li et al. 2017; Bandara et al. 2018). The integration of CNT and GO addresses these issues and introduces CPI as a biodegradable resource (Li et al. 2017). This aligns seamlessly with the growing demand for eco-friendly alternatives across various sectors, such as the wood industry (Antov et al. 2020). Integrating small ratios of CNT and GO into protein-based adhesives offers a more sustainable alternative to formaldehyde-based adhesives (Zhou et al. 2010; Tasis 2015; Bandara et al. 2017b). This approach utilizes biodegradable resources like soy protein, enhancing performance and durability. These nanomaterials significantly improve bio-based adhesives' mechanical strength and resilience, rivaling conventional performance options (Bandara et al. 2017a; Bandara and Wu 2018). This shift represents a move toward environmentally friendly practices in the adhesive industry by reducing reliance on petroleum-based adhesives (Eisen et al. 2020).

However, while CNTs and GO present notable benefits, addressing their potential toxicological impacts is crucial. Studies have indicated that inhalation or prolonged exposure to CNTs may lead to respiratory issues and other health concerns due to their fibrous nature, which shares similarities with asbestos (Aschberger et al. 2010; Castranova et al. 2013; Fatkhutdinova et al. 2015; Fukushima et al. 2018; C. W. Lam et al. 2006). Similarly, GO's potential to induce oxidative stress raises toxicological concerns (Seabra et al. 2014; Rhazouani et al. 2021; Yuan et al. 2021; Yadav et al. 2022). It is important to emphasize that, in the context of adhesives, these nanomaterials are encapsulated within a matrix, significantly reducing the risk of direct exposure (Liu 2005; Prakash et al. 2011). Furthermore, ongoing research and development efforts (Bussy et al. 2013; Saito et al. 2014; Amenta and Aschberger

2015; Kim et al. 2023), which are actively focused on enhancing the safety profiles of CNTs and GO, should provide reassurance about the progress in the field. Additionally, CNTs and GO are not inherently biodegradable, posing challenges to their environmental degradation (Bianco et al. 2011; Bellanthudawa et al. 2023). However, incorporating them in a small amount into biodegradable matrices, such as CPI, offers a potential solution. The biodegradable nature of proteins like CPI can help mitigate the persistence of these nanomaterials in the environment (Ong et al. 2010).

Despite these challenges, using CNTs and GO in adhesives contributes to eco-friendliness in several ways. Firstly, by enhancing the performance and longevity of the materials they bond (Guadagno et al. 2014; Bandara et al. 2017b), these nanocomposites reduce the need for frequent replacements, ultimately conserving resources. In addition, their ability to improve adhesive properties without relying on harmful formaldehyde-based alternatives translates to safer indoor air quality and healthier living environments (Istek et al. 2018; Zhang et al. 2018).

Studies demonstrate that incorporating CNTs and GO into protein adhesives significantly enhances their tensile strength, shear strength, and toughness (Guadagno et al. 2014). These nanomaterials act as reinforcing agents by effectively transferring stress within the adhesive matrix. For instance, Bandara et al. (2017a) found that the integration of GO remarkedly increased the adhesive's bonding strength. Consequently, even minor additions (up to 1% by weight) of graphene to epoxy adhesives have been shown to enhance joint strength significantly (Guadagno et al. 2014), indicating that high surface area and unique interfacial interactions of nanomaterials can contribute to stronger adhesion between the adhesive and wood substrates. Further enhancing their performance, CNTs and GO can also exhibit hydrophobic properties, improving water resistance (a critical factor for wood adhesives) in the final adhesive, where moisture can severely compromise bond integrity. Notably, GO has been shown to improve the water resistance of a canola protein-based adhesive (Bandara et al. 2017b).

This research underscores the potential of CNT and GO nanocomposites as sustainable alternatives to conventional formaldehyde-based wood adhesives. By leveraging the unique properties of these nanomaterials and incorporating them into a biodegradable CPI matrix, this study paves the way for environmentally friendly adhesives with enhanced performance properties. While toxicological and biodegradability concerns warrant further investigation, the potential benefits of these nanocomposite bioadhesives, including reduced formaldehyde emissions, improved bonding strength, and water resistance, position them as a promising solution for a more sustainable future in the wood industry. Further research should focus on optimizing synthesis parameters, properly dispersion of nanomaterials into protein matrix, and conducting comprehensive life cycle assessments of these adhesives.

Experimental section

Materials and chemicals

The discarded cold screwed-pressed canola meal (CM), containing 38% protein and 10% moisture content, was obtained from Southern Oil (Pty) Ltd in Swellendam, South Africa. Chemicals, such as analytically graded hexane, NaOH (≥98%), HCl, H_2SO_4, and 55% HNO_3 with approximately 99% purity, were procured from Rochelle Chemicals in Johannesburg, South Africa. N_2 and C_2H_2 gases were purchased from Afrox in Booysens, South Africa. Additionally, maple wood was acquired from H & S Timber Company in Benoni, South Africa, and veneer samples were crafted with dimensions of 55 × 130 × 6 mm (width × length × thickness).

Methods

Extraction of CPI from the CM

The extraction method employed for extracting CPI from CM (the residue remaining after oil extraction from canola seeds) was slightly modified from the process outlined by Bandara and Wu (2018). In summary, the CM was oven-dried at 49 °C for 24 h to remove moisture. Subsequently, it was crushed into a powder using a pulverizer to achieve a finely particulate size using a 0.50 mm mesh sieve. The

defatting (involving fat removal) was done at room temperature by washing the crushed CM with hexane at 1:10 (w/v). This defatting process was performed four times until a minimal fat was observed through the texture and appearance of the sample. To further eliminate excessive hexane, the defatted CM oven-dried at 40 °C for 10 h.

For CPI extraction, the defatted CM was mixed with milli-Q water at a 1:10 (w/v) ratio and stirred for 40 min using a magnetic stirrer to form a well-dispersed mixture. The pH of the mixture was raised from 6.7 to 12.0 using 3 M NaOH, followed by another 2 h of stirring to solubilize the proteins, facilitating their segregation from other components. Centrifugation at 6000 RPM for 15 min separated the solid and liquid components of the CM mixture and the supernatant collected. To precipitate proteins, the pH of the supernatant was adjusted from 12.0 to 4.0 with 3 M HCl, then stirred for 20 min with a magnetic stirrer to isolate the protein and centrifuged at 6000 RPM for 15 min to extract the CPI. The precipitate (CPI) was collected and subjected to four washes with milli-Q water to eliminate impurities. The extracted CPI, constituting approximately 37% w/w of the CM, was used as an adhesive, with some freeze-dried for later use.

Catalyst preparation for CNT synthesis

A catalyst comprising iron and cobalt (Fe-Co) was synthesized through the wet impregnation method on a substrate composed of calcium carbonate, following the procedure outlined by Mhlanga and Coville (2008) with some minor adjustments. In summary, 3.62 g of iron nitrate and 2.47 g of cobalt nitrate were finely ground, combined with 30 mL of distilled water, and subjected to magnetic stirring for 20 min to create the Fe-Co nitrate solution. Separately, 10 g of $CaCO_3$ was placed in a beaker, and 30 mL of the previously prepared Fe-Co nitrate solution was gradually added, followed by stirring for 45 min. The resulting solution was filtered, dried for 12 h at 120 °C in an air oven, and cooled to room temperature. The dried material was pulverized and sifted through a 0.15 mm sieve, then calcinated for 16 h at 400 °C.

Synthesis of CNT using the chemical vapor deposition (CVD) method

The CNT was produced by decomposing acetylene gas on a Fe-Co catalyst within a high-temperature furnace in a CVD reactor, following the method outlined by Mhlanga et al. (2009) with minor adjustments. A ceramic boat (120 mm × 15 mm) containing 1 g of the Fe-Co catalyst was placed inside the CVD furnace in a horizontal quartz tube (51 cm × 1.9 cm). The furnace was heated at a rate of 10 °C/min. Nitrogen purging commenced immediately after heating, with a 30 ml/min flow rate through the quartz tube and the catalyst. Upon reaching 700 °C, the nitrogen flow rate was increased to 230 ml/min, and acetylene gas was introduced at 190 ml/min. The reaction proceeded for 60 min at a constant temperature of 700 °C. Subsequently, the acetylene supply was halted, and the furnace was allowed to cool to room temperature under a continuous nitrogen flow. The resulting CNTs were collected, and their yield was determined by weighing the product with a weighing balance.

Synthesis of graphene oxide

With slight adjustments, GO was synthesized following the Hummers and Offeman method (Chen et al. 2013). Briefly, 5 g of graphite and 5 g of $NaNO_3$ were combined in a glass beaker. Subsequently, 120 mL of concentrated H_2SO_4 was gradually introduced while stirring in an ice bath at 200 RPM for 2 h. Then, 15 g of $KMnO_4$ was progressively introduced into the reaction mixture, maintaining the temperature at 35 ± 3 °C with stirring for an additional 1 h. To terminate the reaction, 92 mL of deionized water was added and stirred for 15 min. Any unreacted KMnO4 and residual chemicals were neutralized by introducing 80 mL of hot (60 °C) deionized water containing 3% H_2O_2. After cooling to room temperature, the mixture underwent centrifugation (10000×*g*, 15 m, 4 °C) and subsequent washing with deionized water to eliminate any remaining chemicals. The collected GO samples underwent sonication for 5 m (at 50% power output), followed by freeze-drying, additional drying in a vacuum desiccator with P_2O_5, and stored in air-tight containers for further use.

Fabrication of nanocomposite bio-adhesives through the incorporation of nanomaterials

Incorporating CNTs in the CPI was carried out following the method by Bandara and Wu (2018) with some modifications. In summary, 20% w/v (CPI/H_20) dispersions were prepared by combining 2 g of CPI with 10 ml of milli-Q water in five separate beakers. To ensure an even distribution of the CPI, the solutions were agitated for 3 h at 300 rpm and room temperature, after which 1 M HCl solution was used to adjust the pH to 5. Then, various concentrations (0.5/0.5%, 0.7/0.3, 0.3/0.7%, 0.9/0.1%, 0.1/0.9 w/w) of CNT/GO, respectively, were added. The mixture was agitated for 2 h at 300 rpm, maintaining the temperature at 27 ± 2 °C, followed by an additional 1 h at 45 ± 1 °C using a temperature-controlled stir plate and a thermometer to monitor the temperature change. A high-intensity ultrasonicator (UCP − 10 model, Apex scientific) was used to sonicate the CPI nanomaterials at 50% power output for 3 min. A high shear homogenizer (FJ200-SH model, Masiye labs) was employed to homogenize the resulting mixtures for 2 min at 20,000 rpm. After the dispersion to form nanocomposite adhesives, the pH was readjusted to 12 with 6 M NaOH, followed by further sonication and homogenization with the same conditions above.

The final product of the adhesive was brownish in color, with a final solid content of approximately 28% w/v. The viscosity was approximately 988 ± 12 cps. The shelf life could not be determined but recommended for future study.

Wood surface treatment and adhesive sample application

Maple hardwood (density of 0.042 g/cm^3) with a moisture content of approximately 11% was used as the wood substrate. Ensuring proper adhesion between the adhesive and the wood involves meticulous surface treatment using 80-grit sandpaper to achieve a fine and smooth texture. Any residual oil or dirt on the wood surfaces was removed by wiping with a cloth dampened in acetone.

The prepared adhesive samples were precisely applied using a micropipette at an amount of 40 µL per veneer strand over a contact area of 40 mm × 100 mm (width × length). Three bonded replicate samples were prepared. Another piece of wood was then firmly bonded to the adhesive-applied end, ensuring an application area of 30 mm × 25 mm. The assembly was pressed in a hydraulic press (Model 3890 Auto M hot press) under conditions of 1.4 MPa and 180 °C for 10 min.

After the adhesive process, the assembled wood samples, each weighing 10 g, underwent a curing period of 3 days in a climatic chamber maintained at 25 °C and 50% relative humidity (RH) (Balmori et al. 2021).

Assessment of adhesive strength and water resistance

A tensile shear test was used for the evaluation of adhesive (bond) strength. The tensile testing machine (AG-IC 20/50 kN Shimadzu, 346-54411-51) with a 20 kN load cell, operated at a crosshead speed of 1.0 mm/min, was utilized. The shear strength at the maximum load point, corresponding to the maximum force applied to break the bonded wood samples, was determined using Equation 1. These values were calculated based on the average measurements obtained from three specimens of the same adhesive sample. The shear strength assessments included three distinct tests: dry, wet, and soak shear strengths, conducted under the European standard for adhesive testing.

$$Pressure(Pa) = \frac{\text{Force(N)}}{\text{Area}(m^2)} \quad (1)$$

Assessment of shear strength under dry, wet, and soak conditions

The bonded wood samples underwent a seven-day drying period in a climate chamber set at 25 °C and 50% RH. Subsequently, bond strength was evaluated following the European standard (EN-204) for interior durability class D1. For the wet shear strength test, aligning with EN-204 durability class D2, the adhesive wood samples were immersed in tap water for 3 h before testing. To determine soak shear strength, the adhesive wood samples were soaked in tap water for two days and then conditioned for an additional seven days in a climate chamber at 25 °C and 50% RH under EN-204 durability class D2 guidelines (Šljivo et al. 2023). Refer to Table 1 for detailed procedures.

Table 1. The durability classes follow the European interior wood standard (EN-204).

Conditioning procedure	Shear strength (MPa)	Durability classes
7 days in a standard atmosphere	≥10	D1
Seven days in standard atmosphere, 3 h in water at (20 ± 3 °C), and 7 days in standard atmosphere.	≥8	D2

Table 2. Composition of defatted canola meal (Barzegar et al. 2020).

Components	Percentage (%)
Protein ($N \times 6.25$)	35
Carbohydrates	35
Remaining Fat	2
Ash	6
Other materials (Glucosinolates, erucic acid, phytic acid, phenolics, etc., in canola flour., the fiber in soy flour)	22

Evaluation of morphological properties using SEM

Scanning Electron Microscopy (SEM) was employed to examine the morphological properties (the structure and interactions within the sample matrices) of the nanomaterials and the nanocomposite adhesive samples. To mitigate charging during the analysis, a coating of 60% palladium and 40% gold (Pd/Au) was applied to the samples.

Fractured wood adhesive samples were achieved by bonding two wooden pieces with the adhesive. After allowing the sample to dry based on the testing condition, mechanical testing resulted in sample fracture. A cross-sectional view of the fracture was then obtained for SEM analysis.

Evaluation of thermal properties using TGA

To assess the thermal stability, a TA SDT Q600 thermogravimetric analyzer (DRYCAL TA) with nitrogen gas set at 10 mL/min was used. Freeze-dried adhesive samples, each weighing approximately 5.0 mg, were individually placed in alumina pans. The temperature ramped from room temperature to 800 °C, and data were automatically generated and plotted.

Evaluation of crystalline structure using X-ray diffraction

A Rigaku Ultima IV powder diffractometer performed X-ray diffraction (XRD) on the samples. Data for glancing angles (2θ) between 5 and 50° were obtained using Cu-K radiation at 0.154 nm. Bragg's equation was applied to determine the interlayer spacing (d) of the samples. The XRD data were analyzed using an Origin plot.

Evaluation of functional groups using FTIR

Fourier Transform Infrared (FTIR) Spectroscopy was employed to assess the attachment and types of functional groups on the samples' surfaces. Briefly, approximately 2 mg of dried powder samples were measured into the infrared analyzer (Bruker Tensor 27). Spectra were obtained in the range of 500–5000 cm^{-1}.

Statistical analysis

The effects of the nanomaterials on dry, wet, and soak adhesive strengths were assessed using Fisher's analysis of variance and Duncan's multiple-range test. Data were collected at a 95% confidence level (Sagala et al. 2023).

Results and discussion

Evaluation of the protein content

Protein Content Assessment: The protein content within the CM was assessed using a PerkinElmer Model 2400 Series II CHNS/O Analyzer. The nitrogen percentage obtained was converted into protein percentage by applying a factor of 6.25, assuming that proteins contain approximately 16% nitrogen (Mariotti et al. 2008). The analysis focused on the extracted CPI sample, which exhibited a nitrogen content of 5.95%. Multiplying this figure by the conversion factor yielded a protein percentage of 37.2%. In contrast, Barzegar et al. (2020) reported a 35% protein recovery from CM (Table 2), suggesting an enhancement in the current study. Other constituents of CM were not examined or disclosed in this research.

Raman spectra of graphene oxide and carbon nanotube

The Raman spectra of the pristine GO, as shown in Figure 1a, exhibited the D and G bands at 1351 cm^{-1} and 1598 cm^{-1}, respectively. The D band is attributed to structural defects and disorder, while the G band arises from the in-plane stretching motion of sp^2 carbon atoms. The smaller peak at 2949 cm^{-1} is associated with the presence of functional groups in the GO, such as carboxyl groups (Aregahegn Dubale et al. 2014). López-Díaz et al. (2020) reported similar peaks of GO and reduced graphene oxide (rGO) at 1350 and 1585 cm^{-1} for the D and G bands respectively. studies have shown that the Raman spectra of GO's characteristic peaks can provide insights into their structural and chemical properties. The intensities of the D and G bands, as well as additional peaks, can vary depending on the degree of oxidation, the presence of functional groups, and the method of synthesis (Johra et al. 2014; Muzyka et al. 2018).

Figure 1b shows the Raman spectra of the CNT, the absence of the radial breathing mode (RBM) designates the presence of Multi-Walled Carbon Nanotubes (MWCNT), also the peaks align with the ones observed in a previous study on MWCNT by Bai et al. (2016). The D-band at 1359 cm^{-1} signified the existence of sp3 hybridized carbon atoms, along with structural defects or disorder in the carbon system of the MWCNTs. Additionally, the G-band at 1359.44 cm^{-1} and G'-band at 1590.36 cm^{-1} originated from the in-plane vibration and out-of-plane symmetry modes of the graphitic lattice of the MWCNTs, respectively. Furthermore, the peak at 2699 cm^{-1} corresponds to the G'-band, resulting from a second-order scattering process involving two phonons. This peak is sensitive to the stacking order of the graphene layers in the CNT structure, providing insights into the number of graphene layers present. In single-walled carbon nanotubes (SWCNT), this peak is typically absent or very weak.

The effect of the concentration of CNT and GO hybrid on the adhesive strength of the nanocomposite adhesives

Figure 2 presents the adhesive strengths of the nanocomposite adhesive under different percentages of CNT/GO (C/G) concentrations at w/w CPI in three states: dry, wet, and soaked. Generally, adhesive strength increases with the concentration of CNT and GO up to a certain threshold. For instance, comparing the adhesive strength of the pristine CPI to 0.5/0.5% reveals a notable increase in all states. However, the trend is not strictly linear; for example, at 0.7/0.3%, the adhesive strength in the dry state is lower than at 0.5/0.5% despite a higher CNT concentration.

Wet and soaked states consistently show higher adhesive strengths than the dry state, suggesting improved performance under moist conditions. The highest adhesive strength was observed at concentrations of 0.5/0.5% in the dry state and 0.3/0.7% in the wet/soaked states, correlating with the wood failure rates. These results suggest that an optimal CNT GO ratio maximizes adhesive performance, and exceeding this ratio can lead to diminished bonding effectiveness.

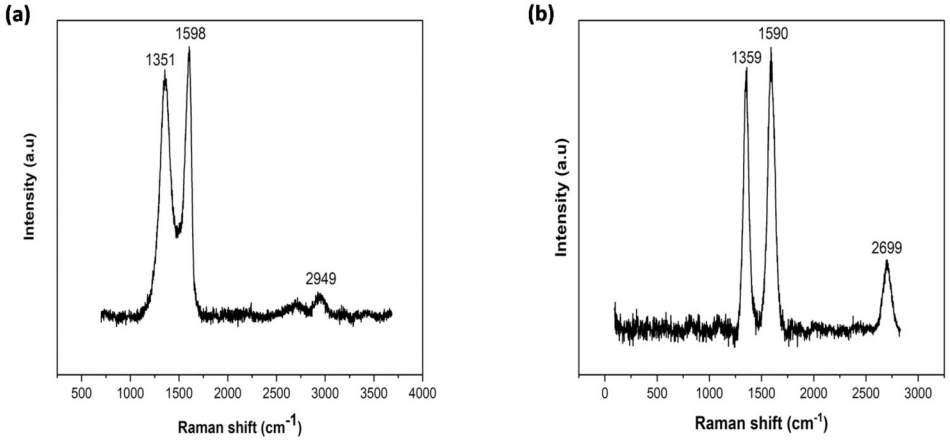

Figure 1. Raman spectra showing different peaks of pristine: (a) graphene oxide and (b) carbon nanotube.

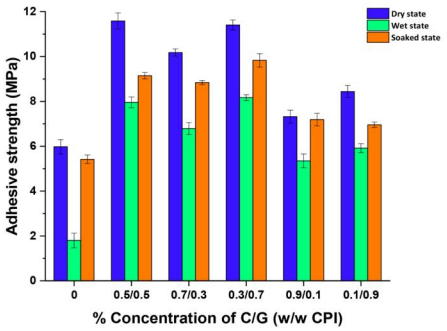

% concentration of C/G w/w CPI	Wood failure rate (%)
0	45.7
0.5/0.5	70.2
0.7/0.3	68.1
0.3/0.7	59.4
0.9/0.1	51.6
0.1/0.9	63.4

Figure 2. The adhesive strengths of the adhesive samples at different states and concentrations, including a table (on the right) presenting the wood failure rate at different adhesive concentrations.

Similarly, the wood failure rate, as shown in the Table below, reflects this trend. The wood failure rate (%) increases from 45.7% for the pristine CPI (0% C/G) to a maximum of 70.2% at 0.5/0.5% C/G concentration, indicating enhanced bonding performance with the addition of CNT and GO. However, the wood failure rate decreases beyond this optimal ratio. For example, at 0.7/0.3% C/G, the wood failure rate slightly drops to 68.1%, and further decreases are observed at 0.9/0.1% (51.6%) and 0.3/0.7% (59.4%).

A recent study by Sun et al. (2021) demonstrated that incorporating a blend of CNT and GO can improve the mechanical properties of polymers. In this approach, three-dimensional (3D) GO aerogels serve as effective carriers for CNT, ensuring their uniform dispersion and subsequent incorporation into the polymer matrix. This addresses the challenge of poor dispersion commonly encountered when integrating CNT into polymers. Another study by Tripathi et al. (2020) highlighted the potential of free-standing GO and CNT hybrid papers to improve mechanical and electrical performance when used in conjunction with polymer laminates. Nevertheless, despite these promising results, a comprehensive understanding of the effect of the concentration of the CNT and GO hybrid on polymer performance requires further research.

Effect of CNT and GO hybrid on the structural changes of the CPI

Figure 3 showcases the FTIR spectra of the CPI enhanced with varying ratios of CNT and GO, providing profound insights into the nanocomposite's functional groups and the protein's secondary structures. The observed peaks at different wavenumbers are significant, as they offer a deep understanding of the intricate interactions between the nanomaterials and CPI. This elucidates how the incorporation of CNT and GO influences the composite's molecular characteristics. In Figure 3a, CPI exhibits distinct peaks at 2850–2920 cm^{-1}, corresponding to the C–H stretching vibrations of aliphatic groups, and at 1650 cm^{-1} and 1550 cm^{-1}, which are associated with the amide I and II bands, respectively. These peaks signify the preservation of the protein's backbone and secondary structure, indicating that the fundamental protein conformation remains intact (Gbassi et al. 2012).

Moving on to spectrum (b), CNT displays a broad peak around 1600 cm^{-1} attributed to the C = C stretching of sp^2-hybridized carbon networks. This confirms the intact conjugated structure of the CNTs within the composite, implying that the CNTs maintain their structural integrity and electronic properties when incorporated with the protein (Azri et al. 2017). Similarly, spectrum (c) for GO shows characteristic peaks at 3200–3600 cm^{-1} due to O–H stretching vibrations, 1720 cm^{-1} corresponding to C = O stretching, and 1000–1300 cm^{-1} associated with C–O stretching vibrations. These indicate the successful oxidation of graphene, also confirming and enhancing its bonding capability with CPI, as these oxygen-containing functional groups on GO facilitate stronger interactions with the protein matrix (Manoratne et al. 2017).

Moreover, in Figure 3d, the spectral regions from 4000 to 3200 cm^{-1} and from 2700 to 1800 cm^{-1}

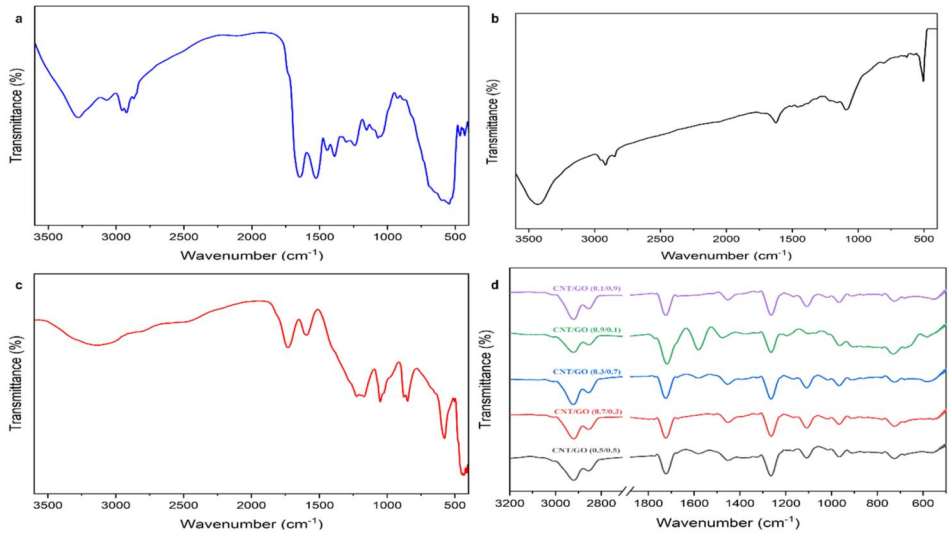

Figure 3. FTIR spectra of the (a) CPI, (b) CNT, (c) GO, and (d) CPI adhesive samples with varying ratios of CNT and GO showing some uniform and distinct peaks.

were omitted as they contain no significant information and enable visibility of the relevant peaks. Notably, the peak at 724 cm^{-1} does not provide detailed information about the samples' functional groups or secondary structures; instead, it indicates the presence of CNT or related carbon-based materials within the samples.

Further peaks at 2852 cm^{-1} and 2924 cm^{-1} correspond to the stretching vibrations of the C–H bonds in the protein, likely arising from aliphatic groups. Additionally, the peaks at 1451 cm^{-1} and 1723 cm^{-1} are attributed to the asymmetric and symmetric stretching vibrations of the C = O bonds in the CPI, suggesting the existence of carboxylic acid groups. Furthermore, the peaks at 1266 cm^{-1} and 1108 cm^{-1} are associated with the stretching vibrations of the C–N and C–O bonds, respectively, indicating the presence of amide groups within the protein structure. The peak at 968 cm^{-1} corresponds to the bending vibration of the C–H bond, further linking to the presence of aliphatic groups (Bandara et al. 2017a, 2017b; Bandara and Wu 2018).

However, the exceptional peak at 1581 cm^{-1} observed exclusively in the CPI-C/G (0.9/0.1) sample may indicate a specific molecular vibration arising from the interaction between the protein and the nanomaterials at this ratio. This unique spectral feature could signify a stronger interaction between CPI and CNT/GO at this composition, potentially enhancing the nanocomposite's mechanical properties or adhesive strength.

Effect of the nanomaterials on the viscosity of the CPI adhesive

The viscosity of the adhesive nanocomposite was observed to steadily increased with the increase in the ratios of the nanomaterials. This phenomenon stems from the increased interfacial interactions due to the high surface area of these nanomaterials, which enhances resistance to flow (Zheng et al. 2008; Xiao et al. 2015; Ashraf et al. 2018). Furthermore, CNTs and GO can form interconnected networks within the adhesive at certain concentrations, further hindering flow and contributing to a more viscous solution (Meeuw et al. 2018). This increase in viscosity is critical as it affects the adhesive's application and performance, ensuring better spreadability and stronger bonding properties.

The effect of the nanomaterials on the thermal stability of the nanocomposite adhesives

The thermogravimetric analysis (TGA) data presented in Figure 4 provides valuable insights into enhancing thermal stability in CPI adhesives by incorporating CNT and GO. By examining the degradation patterns of the samples, we can better understand the mechanisms underlying the composite material's improved thermal properties. Notably, an intriguing observation in the CNT data is the apparent weight gain between 30 °C and 250 °C, which warrants further investigation

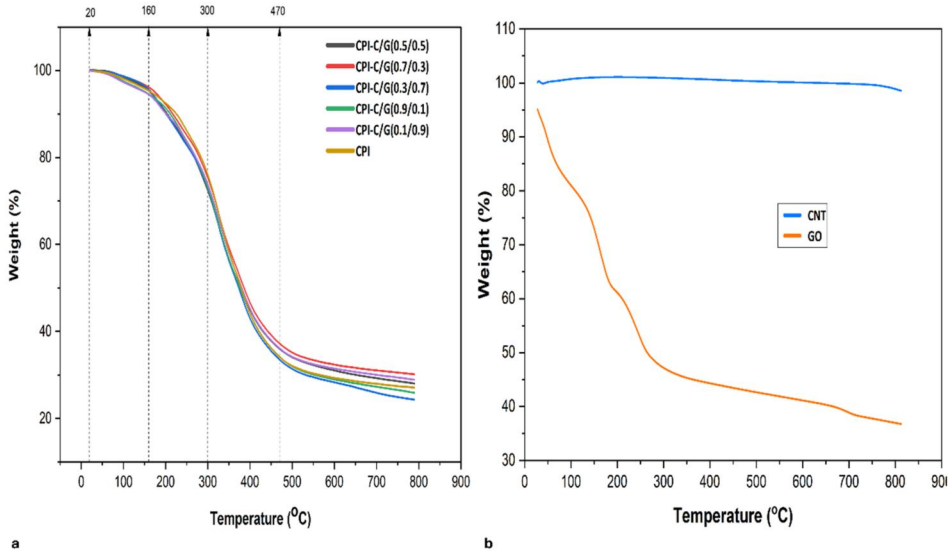

Figure 4. Thermogravimetric analysis (TGA) of; (a) CPI and nanocomposite adhesive samples, (b) CNT and GO.

(Figure 4b). This weight gain can be attributed to several factors, such as moisture adsorption. Due to their high surface area and porous structure, CNTs are prone to adsorbing water molecules from the environment (Gangupomu et al. 2016).

The pristine CPI exhibits significant and rapid weight loss as the temperature increases, indicative of its limited thermal stability (Figure 4a). This rapid degradation is characteristic of protein-based materials, which tend to decompose at relatively low temperatures due to the breakdown of peptide bonds and side-chain functionalities (Bandara and Wu 2018). In contrast, the CPI composites enhanced with CNT and GO display a slower rate of weight loss, signaling increased resistance to thermal degradation. This improvement suggests that CNT and GO play critical roles in reinforcing the CPI matrix, thereby delaying the decomposition of the protein and other organic components.

The phase-wise thermal degradation analysis further supports the role of CNT and GO in enhancing CPI's thermal stability. In the first phase, between 22 °C and 160 °C, all samples, including the nanocomposites, exhibit minimal weight loss, primarily due to the evaporation of moisture and low-boiling-point volatiles.

In the second phase (160 °C to 470 °C), the rate of weight loss for the nanocomposite adhesives is significantly slower compared to pristine CPI. This decelerated degradation can be attributed to the barrier effect provided by CNT and GO, which stabilizes the protein matrix by shielding it from heat and mass transfer processes that facilitate decomposition. The strong interfacial bonding between the protein chains and the nanomaterials enhances the structural rigidity of the composite, thereby delaying thermal degradation. Moreover, the improved thermal conductivity of CNTs aids in distributing heat more uniformly throughout the material, reducing thermal gradients that can cause localized degradation.

As the temperature rises to the final decomposition phase, from 470 °C to 800 °C, the degradation of residual carbonaceous material becomes prominent. Here, the nanocomposite composites retain more weight compared to pure CPI, underscoring the stabilizing effect of CNT and GO.

The morphological analysis of the nanomaterials and adhesive samples

Figure 5 presents SEM images describing the CNT and GO at various magnifications. The CNT displays an average outer diameter of 98.8 ± 2 nm (Figure 5a), corresponding to the range reported by Mhlanga and Coville (2008). Notably, the CNT exhibits a significant number of clusters, amorphous carbon, and other impurities, likely originating from the partial or incomplete nucleation of carbon atoms during the synthesis process (Little 2003). These clusters imply potential interactions and agglomeration among the CNTs. Such conditions

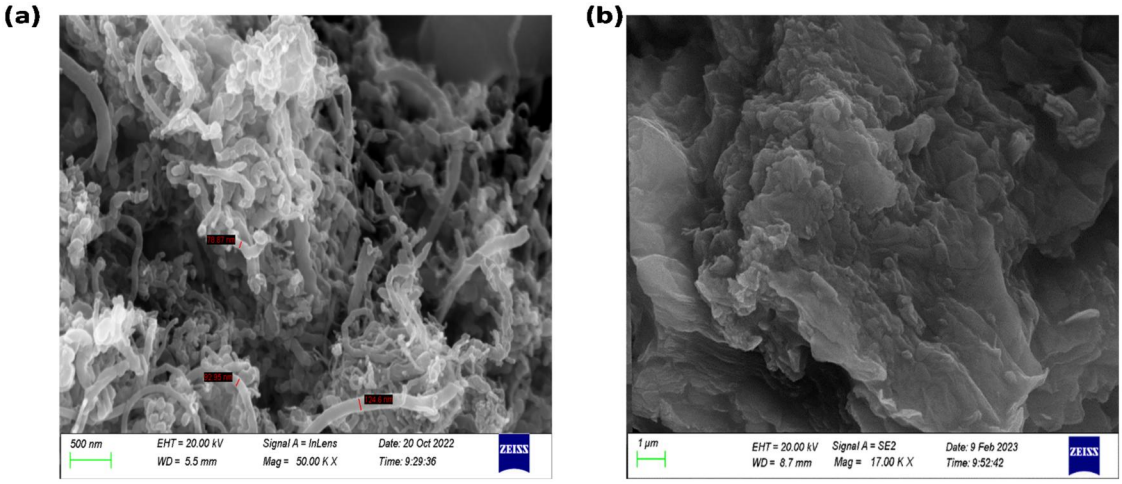

Figure 5. The SEM image of: (a) CNT and (GO) at different magnifications.

can alter the materials' properties, offering avenues for tailored applications. The identification of amorphous carbon regions also points to the need for refining the synthesis parameters to minimize impurities and enhance the overall structural integrity of the CNTs. Moreover, the GO sheets (Figure 5b) exhibit a complex and layered arrangement, showcasing a crumpled morphology indicating the presence of oxygen-containing functional groups on the graphene surface. This crumpled structure is a result of the oxidation process during the synthesis of GO, leading to the introduction of various oxygen-based functionalities such as epoxide, hydroxyl, and carboxyl groups. Additionally, oxygen functionalities on the GO sheets impart unique properties and enhance the compatibility and interaction between GO and CNT within the nanocomposites.

Furthermore, the SEM images reveal that all CPI-C/G adhesive samples exhibit rough and porous surface morphologies due to incorporating varying ratios of CNTs and GO (Figure 6). This structural roughness and porosity are introduced by the homogeneous distribution of the nanomaterials, which create structural layering and uneven textures across all samples. Samples with higher GO content, such as CPI-C/G(0.1/0.9) and CPI-C/G(0.3/0.7) shown in Figures 6b and 6d, display more fragmented and highly porous surfaces due to GO's high surface area and abundant functional groups, which improve bonding at the microstructural level but may risk mechanical integrity if not uniformly dispersed (Bandara et al. 2017b). Conversely, samples with higher CNT content, like CPI-C/G(0.7/0.3) and CPI-C/G(0.9/0.1) illustrated in Figures 6c and 6e, present smoother and more compact surfaces with reduced porosity, reflecting the reinforcing nature of CNTs that enhance tensile strength and structural integrity (Ejaz et al. 2022). The consistent presence of roughness and porosity across all samples underscores the significant impact of CNT and GO incorporation on the adhesive's microstructure. Adjusting their ratios to balance flexibility, toughness, and strength as required for specific applications allows for tailored mechanical properties.

Finally, the pristine CPI adhesive exhibits a relatively smooth surface devoid of the fractures and porosity observed in the composite samples (Figure 6f). This indicates that incorporating CNTs and GO significantly alters the adhesive's microstructure. The absence of these nanomaterials means the pure CPI adhesive lacks the enhanced mechanical properties conferred by the nanocomposite adhesives.

The correlation between surface morphology and adhesive strength emphasizes the significance of achieving optimal nanomaterial dispersion and interfacial interactions for improved adhesive performance. Furthermore, the choice of the CNT/GO ratio is crucial, as a disparity may lead to cluster formations and rough surfaces. Attaining the right proportion ensures a harmonious integration of the nanoparticles, optimizing surface morphology and enhancing the overall performance of the protein-based nanocomposite.

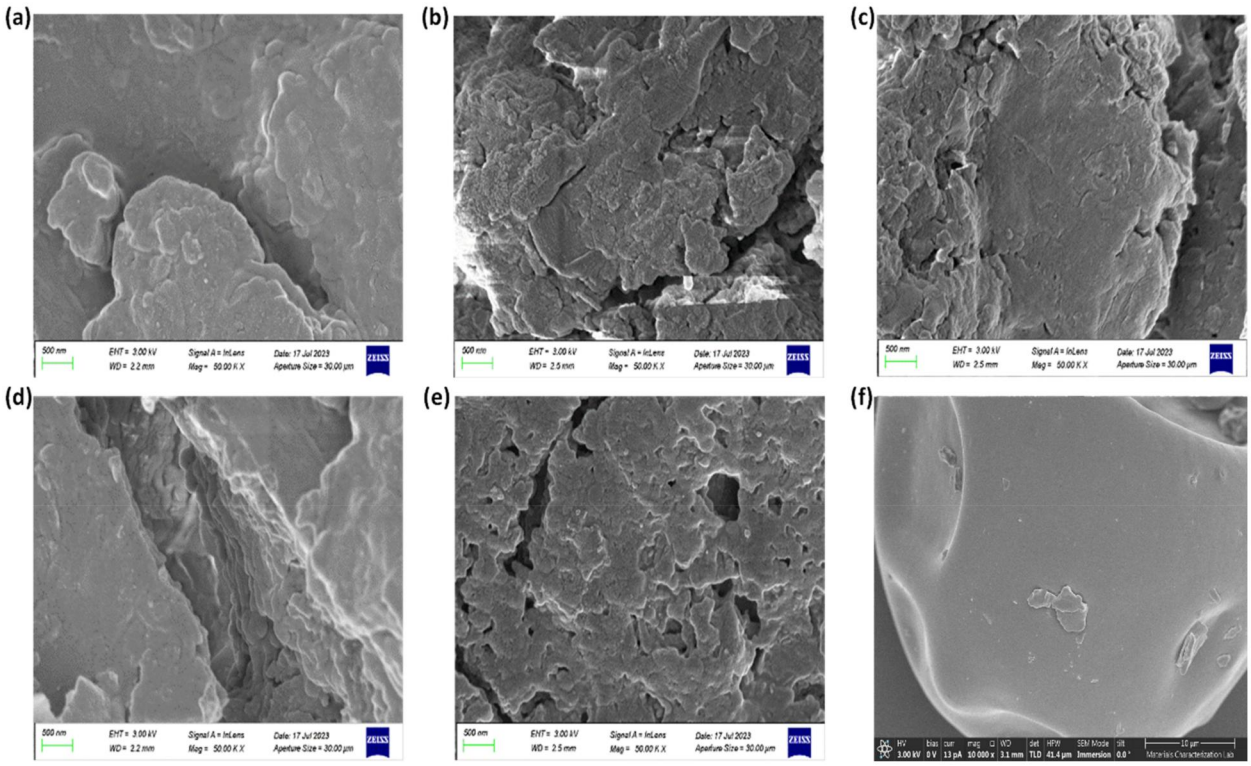

Figure 6. The SEM images of: (a) CPI-C/G(0.5/0.5), (b) CPI-C/G(0.1/0.9), (c) CPI-C/G(0.7/0.3), (d) CPI-C/G(0.3/0.7), (e) CPI-C/G(0.9/0.1), and (f) CPI adhesives.

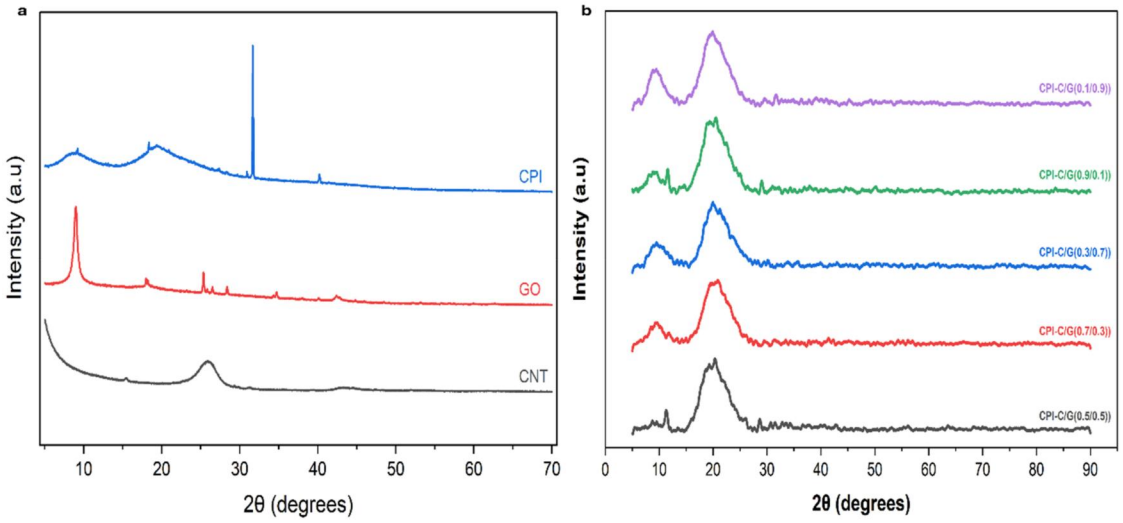

Figure 7. XRD spectra of (a) the CPI, GO, and CNT, (b) the nanocomposite adhesives, showing various peaks and glancing angles (2θ). [notes: the interlayer spacing was determined using Bragg's equation: Sin = n/2d].

Changes in the crystallinity of the nanomaterials and their effect on dispersion in the CPI matrix

The integration of GO and CNT into CPI has significantly enhanced the protein's original structure, as evidenced by changes observed in the XRD patterns. By combining the initial XRD data of CPI, GO, and CNT with the analysis of the enhanced samples (Figure 7), we can understand how these nanomaterials influence the protein's structural properties.

Initially, CPI exhibited XRD peaks at 9.2°, 18.8°, 31.7°, and 40.2°, indicative of its semi-crystalline nature (Figure 7a). These peaks are associated with the periodic arrangements in the protein's secondary and tertiary structures, such as α-helices and β-sheets, reflecting the inherent

folding patterns within the protein matrix (Bandara and Wu 2018; F. Sun et al. 2022).

Upon incorporating GO into the CPI matrix, the XRD patterns show consistent peaks at 9.21°, 11.50°, 20°, and 31.77° across all enhanced samples (Figure 7b). The peak at 9.21°, corresponding to the (001) plane of the hexagonal graphite structure of GO, indicates successful intercalation of GO layers within the protein matrix. This intercalation can improve barrier properties and increase mechanical strength due to GO sheets' high aspect ratio and stiffness. Moreover, the peak at 11.50°, attributed to the (100) plane of GO, suggests an ordered arrangement and alignment of GO sheets within the CPI, enhancing load transfer efficiency between the CPI and GO and contributing to the overall mechanical reinforcement of the composite material.

The presence of the peak at 31.77°, linked to the (002) plane of GO, implies that GO maintains its crystalline structure after integration. This retention is crucial as it ensures that the beneficial properties of GO, such as high thermal stability and electrical conductivity, are imparted to the CPI. The consistent appearance of GO-related peaks indicates strong interactions between the GO sheets and the protein molecules, potentially leading to improved structural stability and enhanced functional properties of the nanocomposite.

Furthermore, the successful addition of CNTs is evidenced by the appearance of a peak at 29°, corresponding to the (002) plane of the hexagonal graphitic structure of CNTs. This peak confirms that CNTs are successfully incorporated into the CPI matrix, potentially enhancing the composite's mechanical properties due to the exceptional strength and flexibility of CNTs. However, the absence of this peak in certain samples, such as CPI-C/G(0.3/0.7) and CPI-C/G(0.7/0.3), suggests variability in the crystalline phase associated with CNTs, likely due to differences in the CNT to GO ratio. Variations in CNT content can affect the dispersion and alignment of CNTs within the composite, influencing the nanocomposite's overall crystalline structure and properties (Sun et al. 2013; Gupta et al. 2016).

These observations align with findings by Sa et al. (2018), who reported that the ratio of CNT to GO significantly impacts the crystalline structure of nanocomposites. The interplay between GO and CNT within the CPI matrix appears to be crucial in determining the material's final properties. A higher ratio of GO may lead to better dispersion of CNTs or even masking of CNT peaks in the XRD patterns. Therefore, controlling the ratios of GO and CNT is essential to maximize the synergistic effects of both nanomaterials on the protein structure.

The morphological structures of the fractured surfaces of the bonded wood samples

Understanding the tendency of these polymers to undergo cohesive failure underscores the importance of reinforcing cohesive interactions for improving the mechanical properties, adhesion, and water resistance of protein-based adhesives. Both GO and CNT exhibit enhanced cohesion after exfoliation into the CPI matrix, indicating that integrating these nanomaterials into the adhesive system contributes to improved bonding and intermolecular interactions. The investigation of the wood-fractured surfaces through SEM, as depicted in Figure 8, provides crucial insights into the nature of adhesive failure. Furthermore, they reveal some distinctions between the wood surfaces bonded with a pristine CPI and those of CPI-C/G adhesives at the same magnifications. The CPI integrated with CNT and GO hybrid show evidence of wood failure due to fiber pulling and breaking, in contrast to the smooth surface observed on the wood surface bonded with the pristine CPI. Analysis suggests that CP-C/G adhesives experience adhesive failure, while the CPI adhesive demonstrates cohesive failure.

Moreover, adhesive failure implies that the bond between the wood substrate adhesive is weaker than the internal strength of the adhesive itself. In contrast, cohesive failure occurs when the adhesive remains intact, but the failure arises within the adhesive material. The observed improvements in cohesive interactions, as evidenced by the adhesive failure in CP-C/G adhesives, are identified as major factors contributing to significantly improved adhesion and water resistance.

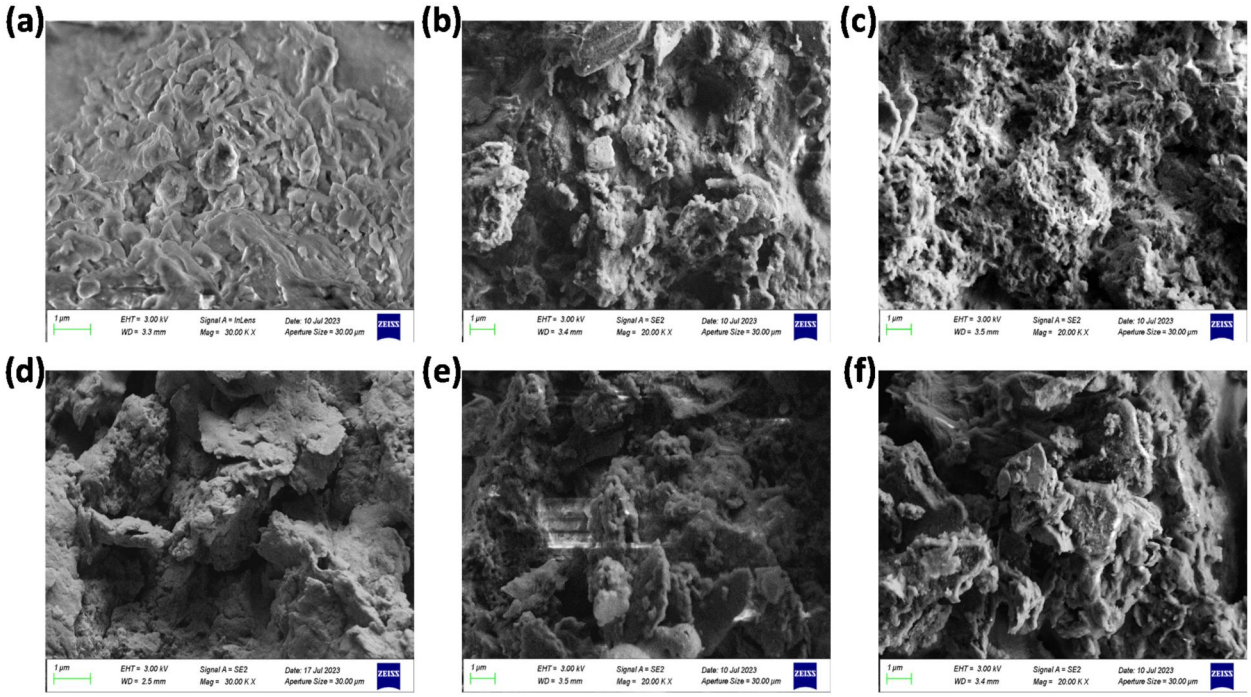

Figure 8. The SEM images of (a) pristine CPI, (b) CPI-C/G(0.5/0.5), (c) CPI-C/G(0.1/0.9), (d) CPI-C/G(0.7/0.3), (e) CPI-C/G(0.3/0.7), (f) CPI-C/G(0.9/0.1) at the same magnification.

Conclusion

This study demonstrates the potential of developing high-performance bio-based wood adhesives by strategically integrating CNTs and GO into a CPI matrix. Tailoring the CNT-GO hybrid ratio enabled the optimization of the adhesive properties under different adhesive states. Notably, a ratio of 0.5/0.5 (CNT/GO) yielded the maximum dry shear strength (11.59 ± 0.36 MPa), while 0.3/0.7 provided the highest wet (8.17 ± 0.13 MPa) and soaked (9.83 ± 0.3 MPa) shear strengths.

Based on our findings, we recommend the adhesive formulation with a CNT/GO ratio of 0.3/0.7 for optimal overall performance. This formulation demonstrated consistently high adhesive strength across dry (9.83 ± 0.30 MPa), wet (8.17 ± 0.13 MPa), and soaked (9.83 ± 0.30 MPa) conditions as per EN-204. While other ratios exhibited peak performance in specific moisture levels, the 0.3/0.7 ratio provides a balanced solution for diverse applications.

Incorporating a CNT/GO hybrid significantly enhances the adhesive strength of nanocomposite adhesives. Notably, the optimal shear strength achieved surpasses that of conventional formaldehyde-based adhesives, specifically phenol–resorcinol–formaldehyde (PRF) and melamine–urea–formaldehyde (MUF), as demonstrated in a study by Liu et al. (2020). While PRF and MUF adhesives exhibit high shear strength at room temperature, their performance deteriorates at elevated temperatures. In contrast, the CPI-CNT/GO hybrid displays better thermal stability, positioning it as a promising alternative to traditional formaldehyde-based adhesives.

The differing performance of CNTs and GO in dry and wet conditions can be attributed to their distinct properties. CNTs are hydrophobic and provide mechanical reinforcement, making them more effective in dry environments where they resist moisture and maintain structural integrity (Xie et al. 2021). Their rigid structure also enhances the adhesive's strength under dry conditions. In contrast, GO is hydrophilic due to its oxygenated functional groups, which allows it to interact with water molecules and maintain adhesive performance in wet or soaked conditions (Hu et al. 2013; Tian et al. 2019). This water interaction enhances GO's dispersion within the adhesive matrix, improving bonding in moist environments. Additionally, the combination of CNTs and GO in a hybrid adhesive leverages the strengths of both materials, with CNTs contributing to mechanical reinforcement in dry conditions, while GO enhances bonding and flexibility

in wet conditions. These synergistic effects explain the optimal CNT/GO ratios observed for different testing conditions.

Limitations of the study

Despite these promising results, this study has certain limitations. Firstly, the study does not address the CPI-CNT-GO adhesive's shelf life or long-term stability. Secondly, while the adhesive is bio-based, the environmental impact of producing CNTs and GO was not covered. Thirdly, the study mentions high viscosity as a drawback of CPI but does not extensively explore how the CNT-GO incorporation affects the adhesive's viscosity and application process. Furthermore, although water resistance is mentioned, further research is necessary to comprehensively understand the adhesive's performance in varying humidity levels and moisture conditions over time. Lastly, a thorough toxicological assessment of the CPI-CNT-GO adhesive is missing.

Future directions

Future research should address these limitations by:

- Investigating the long-term performance and durability of the CPI-CNT-GO adhesive, including accelerated aging tests and real-world application scenarios.
- Conducting a life cycle assessment to evaluate the overall sustainability of the materials used.
- Providing a more detailed analysis of the adhesive's viscosity and application process, considering the influence of CNT-GO incorporation.
- Conducting more extensive testing to assess the consistency and reproducibility of the enhanced mechanical properties across different batches and conditions.
- Performing a comprehensive toxicological assessment to understand any potential health risks associated with the production and use of the CPI-CNT-GO adhesive.
- Exploring other sustainable nanomaterials that could be combined with CPI to enhance adhesive properties while minimizing environmental and health impacts.
- Investigating methods to further enhance the water resistance of the adhesive, potentially through the addition of other hydrophobic nanomaterials or surface treatments.

This research provides a foundation for the development of a sustainable bio-based adhesive by harnessing the synergy between proteins and nanomaterials. Replacing conventional formaldehyde-based adhesives with eco-friendly alternatives will significantly advance sustainability across wood product industries while mitigating health hazards. The framework developed here can be applied to incorporate nanomaterials into other biopolymers to create high-performance green materials for a wide range of engineering applications.

Acknowledgment

The co-authors acknowledge the Penn State Materials Characterization Laboratory for providing access to the FTIR, XRD, TGA, and SEM instrumentation, which were integral to this research. Additionally, we appreciate Jordan Meyet, Nichole Wonderling, Anderson Dean, Zimudzi Tawanda, and Julie Anderson for their valuable insights and guidance on sample preparation.

Disclosure statement

No potential conflict of interest was reported by the authors.

References

Amenta V, Aschberger K. 2015. Carbon nanotubes: potential medical applications and safety concerns. Wiley Interdiscip Rev Nanomed Nanobiotechnol. 7(3):371–386. doi: 10.1002/WNAN.1317.

Antov P, Savov V, Neykov N. 2020. Sustainable bio-based adhesives for eco-friendly wood composites. A review. *Wood Research*, 15. https://d1wqtxts1xzle7.cloudfront.net/62213666/Antov_140320200227-81176-nolv8-with-cover-page-v2.pdf?Expires=1651232488&Signature=ZPO-meiwcTUUMIOwjKBYchGM4aNplPqwA3iArhVDlA9v0CNcPP-MQ8o1mAF4yeExSADT0Pn1C7RzL6Tw2S95VihoORi5W-hV~cDRjZBU35UdWpyT6rNbnCUwjBUfte8kd9~03-23K1UAAOlTszlYhmCjNn0eomrxEwTZ4KkX6lkvfG5PRYH-VdN3Vi6Crv5X9jADmWmSBCWSgg-w1ncRz1LluHtMNaFSPQltzrqy9R73EY8bpi22~18LWLNvGpdqS84lZjqxXXZzCb~~atLayNqf880MZhd8h6d~AEuOziYQtGQieUtIi1qh8sDMoSXeo2jFqkXtNVzRALLqI6muyMsQ__&Key-Pair-Id=APKAJLOHF5GGSLRBV4ZA.

Aregahegn Dubale A, Su W-N, Gedamu Tamirat A, Pan C-J, Asefa Aragaw B, Chen C-H, Hwang B-J. 2014. *Synergetic effect of Graphene on Cu2O Nanowire arrays as highly efficient hydrogen evolution photocathode in water splitting*.

Aschberger K, Johnston HJ, Stone V, Aitken RJ, Hankin SM, Peters SAK, Tran CL, Christensen FM. 2010. Review of carbon nanotubes toxicity and exposure—Appraisal of human health risk assessment based on open literature. Crit Rev Toxicol. 40(9):759–790. doi: 10.3109/10408444.2010.506638.

Ashraf MA, Peng W, Zare Y, Rhee KY. 2018. Effects of size and aggregation/agglomeration of nanoparticles on the interfacial/interphase properties and tensile strength of polymer nanocomposites. Nanoscale Res Lett. 13(1):214. doi: 10.1186/s11671-018-2624-0.

Azri FA, Sukor R, Hajian R, Yusof NA, Bakar FA, Selamat J. 2017. Modification strategy of screen-printed carbon electrode with functionalized multi-walled carbon nanotube and chitosan matrix for biosensor development. Asian J Chemistry. 29(1):31–36. doi: 10.14233/ajchem.2017.20104.

Bai W, Raghavendra A, Podila R, Brown JM. 2016. Defect density in multiwalled carbon nanotubes influences ovalbumin adsorption and promotes macrophage activation and CD4+ T-cell proliferation. Int J Nanomedicine. 11:4357–4371. doi: 10.2147/IJN.S111029.

Bakhtiari SSE, Bakhsheshi-Rad HR, Karbasi S, Tavakoli M, Razzaghi M, Ismail AF, Ramakrishna S, Berto F. 2020. Polymethyl methacrylate-based bone cements containing carbon nanotubes and graphene oxide: an overview of physical, mechanical, and biological properties. Polymers (Basel). 12(7):1469. doi: 10.3390/POLYM12071469.

Balmori JA, Branco JM, Basterra LA. 2021. Behaviour of the adhesive bond between low-grade wood and GFRP reinforcements using epoxy resin. Constr Build Mater. 271:121516. doi: 10.1016/j.conbuildmat.2020.121516.

Bandara N, Akbari A, Esparza Y, Wu J. 2018. Canola protein: a promising protein source for delivery, adhesive, and material applications. J Americ Oil Chem Soc. 95(8):1075–1090. doi: 10.1002/aocs.12039.

Bandara N, Esparza Y, Wu J. 2017a. Exfoliating nanomaterials in canola protein derived adhesive improves strength and water resistance. RSC Adv. 7(11):6743–6752. doi: 10.1039/C6RA27470F.

Bandara N, Esparza Y, Wu J. 2017b. Graphite oxide improves adhesion and water resistance of canola protein–graphite oxide hybrid adhesive. Sci Rep. 7(1):11538. doi: 10.1038/s41598-017-11966-8.

Bandara N, Wu J. 2018. Chemically modified canola protein-nanomaterial hybrid adhesive shows improved adhesion and water resistance. ACS Sustain Chem Eng. 6(1):1152–1161. doi: 10.1021/acssuschemeng.7b03457.

Barzegar M, Behrooz R, Mansouri HR, Najafi SK, Lorenz LF, Frihart CR. 2020. Comparison of Canola and Soy flour with added isocyanate as wood adhesives. J Americ Oil Chem Soc. 97(12):1371–1383. doi: 10.1002/aocs.12410.

Bellanthudawa BKA, Nawalage NMSK, Handapangoda HMAK, Suvendran S, Wijayasenarathne KASH, Rathnasuriya MLD, Wickramasinghe PGMU, Aberathna AAAU, Tennakoon A, Perera IJJUN. 2023. A perspective on biodegradable and non-biodegradable nanoparticles in industrial sectors: applications, challenges, and future prospects. Nanotechnol Environ Eng. 8(4):975–1013. doi: 10.1007/s41204-023-00344-7.

Bianco A, Kostarelos K, Prato M. 2011. Making carbon nanotubes biocompatible and biodegradable. Chem Commun (Camb). 47(37):10182–10188. doi: 10.1039/C1CC13011K.

Bussy C, Ali-Boucetta H, Kostarelos K. 2013. Safety considerations for graphene: lessons learnt from carbon nanotubes. Acc Chem Res. 46(3):692–701. doi: 10.1021/AR300199E/ASSET/IMAGES/LARGE/AR-2012-00199E_0006.JPEG.

Castranova V, Schulte PA, Zumwalde RD. 2013. Occupational nanosafety considerations for carbon nanotubes and carbon nanofibers. Acc Chem Res. 46(3):642–649. doi: 10.1021/AR300004A/ASSET/IMAGES/LARGE/AR-2012-00004A_0002.JPEG.

Chrobak J, Iłowska J, Chrobok A. 2022. Formaldehyde-free resins for the wood-based panel industry: alternatives to formaldehyde and novel hardeners. Molecules. 27(15):4862. doi: 10.3390/MOLECULES27154862.

Dan S, Pant M, Kaur T, Pant S. 2020. Toxic effect of formaldehyde: a systematic review. Int Res J Modern Eng Technol Sci. 179:2582–5208. https://philpapers.org/rec/DANTEO-25.

Dugheri S, Massi D, Mucci N, Marrubini G, Cappelli G, Speltini A, Bonferoni MC, Arcangeli G. 2021. Exposure to airborne formaldehyde: sampling and analytical methods—A review. Trends Environ Anal Chem. 29:e00116. doi: 10.1016/j.teac.2021.e00116.

Eisen A, Bussa M, Röder H. 2020. A review of environmental assessments of biobased against petrochemical adhesives. J Cleaner Prod. 277:124277. doi: 10.1016/j.jclepro.2020.124277.

Ejaz H, Mubashar A, Uddin E, Ali Z, Arif N. 2022. Influence of MWCNTs on strength properties of high viscous epoxy adhesive and fracture behavior of adhesively bonded joints. Theor Appl Fract Mech. 120:103412. doi: 10.1016/j.tafmec.2022.103412.

Fatkhutdinova LM, Khaliullin TO, Shvedova AA. 2015. Carbon nanotubes exposure risk assessment: from toxicology to epidemiologic studies (Overview of the current problem). Nanotechnol Russ. 10(5):501–509. doi: 10.1134/S1995078015030064/METRICS.

Fukushima S, Kasai T, Umeda Y, Ohnishi M, Sasaki T, Matsumoto M. 2018. Carcinogenicity of multi-walled carbon nanotubes: challenging issue on hazard assessment. J Occup Health. 60(1):10–30. doi: 10.1539/JOH.17-0102-RA.

Gangupomu RH, Sattler ML, Ramirez D. 2016. Comparative study of carbon nanotubes and granular activated carbon: physicochemical properties and adsorption capacities. J Hazard Mater. 302:362–374. doi: 10.1016/J.JHAZMAT.2015.09.002.

Gbassi G, Yolou F, Sarr S, Atheba P, Amin C, Ake M. 2012. Whey proteins analysis in aqueous medium and in artificial gastric and intestinal fluids. Int J Bio Chem Sci. 6(4). doi: 10.4314/ijbcs.v6i4.38. 1828–1837

Gonçalves D, Bordado JM, Marques AC, Dos Santos RG. 2021. Non-formaldehyde, bio-based adhesives for use in wood-based panel manufacturing industry—A review. Polymers (Basel). 13(23):4086. doi: 10.3390/POLYM13234086.

Guadagno L, Vietri U, Sarno M, Raimondo M, Cirillo C, Ciambelli P. 2014. Nanofilled epoxy adhesives for structural applications. AIP Conference Proceedings, 1599(1), 390–393. doi: 10.1063/1.4876860.

Gupta P, Rajput M, Singla N, Kumar V, Lahiri D. 2016. Electric field and current assisted alignment of CNT inside polymer matrix and its effects on electrical and mechanical properties. Polymer. 89:119–127. doi: 10.1016/j.polymer.2016.02.025.

Hu X, Yu Y, Hou W, Zhou J, Song L. 2013. Effects of particle size and pH value on the hydrophilicity of graphene oxide. Appl Surf Sci. 273:118–121. doi: 10.1016/j.apsusc.2013.01.201.

Istek A, Özlüsoylu İ, Murat Onat S, Özlüsoylu Ş, Üniversitesi B, Fakültesi O, Endüstri Mühendisliği Bölümü O. 2018. Formaldehyde emission problems and solution recommendations on wood-based boards. J Bartin Faculty Forestry. 20(2):382–387. doi: 10.24011/barofd.425409.

Johra FT, Lee JW, Jung WG. 2014. Facile and safe graphene preparation on solution based platform. J Ind Eng Chem. 20(5):2883–2887. doi: 10.1016/j.jiec.2013.11.022.

Kausar A, Rafique I, Muhammad B. 2017. Aerospace application of polymer nanocomposite with carbon nanotube, graphite, graphene oxide, and nanoclay. Polymer-Plastic Technol Eng. 56(13):1438–1456. doi: 10.1080/03602559.2016.1276594.

Khan DM, Kausar A, Salman SM. 2016. Exploitation of nanobifiller in polymer/graphene oxide–carbon nanotube, polymer/graphene oxide–nanodiamond, and polymer/graphene oxide–montmorillonite composite: a review. Polymer-Plastic Technol Eng. 55(7):744–768. doi: 10.1080/03602559.2015.1103266.

Kim M, Goerzen D, Jena PV, Zeng E, Pasquali M, Meidl RA, Heller DA. 2023. Human and environmental safety of carbon nanotubes across their life cycle. Nat Rev Mater. 9(1):63–81. 1 doi: 10.1038/s41578-023-00611-8.

Kong HX. 2013. Hybrids of carbon nanotubes and graphene/graphene oxide. Curr Opin Solid State Mater Sci. 17(1):31–37. doi: 10.1016/j.cossms.2012.12.002.

Lam CW, James JT, McCluskey R, Arepalli S, Hunter RL. 2006. A review of carbon nanotube toxicity and assessment of potential occupational and environmental health risks. Crit Rev Toxicol. 36(3):189–217. doi: 10.1080/10408440600570233.

Lam J, Koustas E, Sutton P, Padula AM, Cabana MD, Vesterinen H, Griffiths C, Dickie M, Daniels N, Whitaker E, et al. 2021. Exposure to formaldehyde and asthma outcomes: a systematic review, meta-analysis, and economic assessment. PLoS One. 16(3):e0248258. doi: 10.1371/JOURNAL.PONE.0248258.

Li N, Qi G, Susan Sun X, Wang D. 2017. Canola protein and oil-based wood adhesives. Bio-Based Wood Adhesives. 111–139. doi: 10.1201/9781315369242-4.

Little RB. 2003. Mechanistic aspects of carbon nanotube nucleation and growth. J Cluster Sci. 14(2):135–185. doi: 10.1023/A:1024841621054/METRICS.

Liu P. 2005. Modifications of carbon nanotubes with polymers. Eur Polym J. 41(11):2693–2703. doi: 10.1016/j.eurpolymj.2005.05.017.

Liu J, Yue K, Xu L, Wu J, Chen Z, Wang L, Liu W, Lu W. 2020. Bonding performance of melamine-urea–formaldehyde and phenol-resorcinol–formaldehyde adhesive glulams at elevated temperatures. Int J Adhes Adhes. 98:102500. doi: 10.1016/j.ijadhadh.2019.102500.

López-Díaz D, Delgado-Notario JA, Clericò V, Diez E, Merchán MD, Velázquez MM. 2020. Towards understanding the Raman spectrum of graphene oxide: the effect of the chemical composition. Coatings. 10(6):524. doi: 10.3390/coatings10060524.

Salem MZ, Böhm M. 2013. Formaldehyde from wood. BioResources. 8(3):4775–4790.

Manoratne CH, Rosa SRD, Kottegoda IRM. 2017. XRD-HTA, UV visible, FTIR and SEM interpretation of reduced graphene oxide synthesized from high purity vein graphite. Mat Sci Res India. 14(1):19–30. doi: 10.13005/msri/140104.

Mariotti F, Tomé D, Patureau Mirand P, Ois Mariotti F, Tométom D. 2008. Converting nitrogen into protein—beyond 6.25 and Jones' factors. Crit Rev Food Sci Nutr. 48(2):177–184. doi: 10.1080/10408390701279749.

Meeuw H, Wisniewski VK, Fiedler B. 2018. Frequency or amplitude?—Rheo-electrical characterization of carbon nanoparticle filled epoxy systems. Polymers (Basel). 10(9):999. doi: 10.3390/POLYM10090999.

Mhlanga SD, Coville NJ. 2008. Iron–cobalt catalysts synthesized by a reverse micelle impregnation method for controlled growth of carbon nanotubes. Diamond Relat Mater. 17(7-10):1489–1493. doi: 10.1016/j.diamond.2008.01.049.

Mhlanga S, Witcomb M, Carter R, Mondal KC. 2009. *The effect of synthesis parameters on the catalytic synthesis of multi-walled carbon nanotubes using Fe-Co/CaCO3 catalysts*. Vol 62 (67–76). South African Journal of Chemistry, January.

Muzyka R, Drewniak S, Pustelny T, Chrubasik M, Gryglewicz G. 2018. Characterization of graphite oxide and reduced graphene oxide obtained from different graphite precursors and oxidized by different methods using raman spectroscopy. Materials (Basel). 11(7):1050. doi: 10.3390/MA11071050.

Ong YT, Ahmad AL, Zein SHS, Tan SH. 2010. A review on carbon nanotubes in an environmental protection and

green engineering perspective. Braz J Chem Eng. 27(2): 227–242. doi: 10.1590/S0104-66322010000200002.

Prakash S, Malhotra M, Shao W, Tomaro-Duchesneau C, Abbasi S. 2011. Polymeric nanohybrids and functionalized carbon nanotubes as drug delivery carriers for cancer therapy. Adv Drug Deliv Rev. 63(14-15):1340–1351. doi: 10.1016/J.ADDR.2011.06.013.

Rhazouani A, Gamrani H, El Achaby M, Aziz K, Gebrati L, Uddin MS, Aziz F. 2021. Synthesis and toxicity of graphene oxide nanoparticles: a literature review of in vitro and in vivo studies. Biomed Res Int. 2021(1):5518999–5518919. doi: 10.1155/2021/5518999.

Sa K, Mahakul PC, Subramanyam BVRS, Raiguru J, Das S, Alam I, Mahanandia P. 2018. Effect of reduced graphene oxide-carbon nanotubes hybrid nanofillers in mechanical properties of polymer nanocomposites. IOP Conf Ser: mater Sci Eng. 338(1):012055. doi: 10.1088/1757-899X/338/1/012055.

Sagala, D., Sudaryanti, M., & Prihanani, P. (2023). Growth and yield performance of three peanut cultivars on different watering intervals. Indonesian J Agron. 51(2):155–162. doi: 10.24831/ija.v51i2.45794.

Saito N, Haniu H, Usui Y, Aoki K, Hara K, Takanashi S, Shimizu M, Narita N, Okamoto M, Kobayashi S, et al. 2014. Safe clinical use of carbon nanotubes as innovative biomaterials. Chem Rev. 114(11):6040–6079. doi: 10.1021/CR400341H/ASSET/IMAGES/LARGE/CR-2013-00341H_0031.JPEG.

Salthammer T. 2019. Formaldehyde sources, formaldehyde concentrations and air exchange rates in European housings. Build Environ. 150:219–232. doi: 10.1016/j.buildenv.2018.12.042.

Seabra AB, Paula AJ, De Lima R, Alves OL, Durán N. 2014. Nanotoxicity of graphene and graphene oxide. Chem Res Toxicol. 27(2):159–168. doi: 10.1021/TX400385X/ASSET/IMAGES/LARGE/TX-2013-00385X_0004.JPEG.

Šljivo U, Hasanagić R, Fathi L, Bahmani M. 2023. Comparative analysis of bending strength properties between glued and un-glued finger joints in beech and FIR wood species. IOP Conf Ser: mater Sci Eng. 1298(1): 012011. doi: 10.1088/1757-899X/1298/1/012011.

Solt P, Konnerth J, Gindl-Altmutter W, Kantner W, Moser J, Mitter R, van Herwijnen HWG. 2019. Technological performance of formaldehyde-free adhesive alternatives for particleboard industry. Int J Adhes Adhes. 94:99–131. doi: 10.1016/j.ijadhadh.2019.04.007.

Sun X, Chen T, Yang Z, Peng H. 2013. The alignment of carbon nanotubes: An effective route to extend their excellent properties to macroscopic scale. Acc Chem Res. 46(2):539–549. doi: 10.1021/AR300221R/ASSET/IMAGES/LARGE/AR-2012-00221R_0010.JPEG.

Sun F, Li B, Guo Y, Wang Y, Cheng T, Yang Q, Liu J, Fan Z, Guo Z, Wang Z. 2022. Effects of ultrasonic pretreatment of soybean protein isolate on the binding efficiency, structural changes, and bioavailability of a protein-luteolin nanodelivery system. Ultrason Sonochem. 88:106075. doi: 10.1016/J.ULTSONCH.2022.106075.

Sun Y, Xu H, Zhao Z, Zhang L, Ma L, Zhao G, Song G, Li X. 2021. Investigation of carbon nanotube grafted graphene oxide hybrid aerogel for polystyrene composites with reinforced mechanical performance. Polymers (Basel). 13(5):735. doi: 10.3390/POLYM13050735.

Tasis D. 2015. *Carbon nanotube-polymer composites*. Royal Society of Chemistry. https://books.google.co.za/books?id=2GsoDwAAQBAJ.

Tian J, Wu S, Yin X, Wu W. 2019. Novel preparation of hydrophilic graphene/graphene oxide nanosheets for supercapacitor electrode. Appl Surf Sci. 496:143696. doi: 10.1016/j.apsusc.2019.143696.

Tripathi M, Valentini L, Rong Y, Bon SB, Pantano MF, Speranza G, Guarino R, Novel D, Iacob E, Liu W, et al. 2020. Free-standing graphene oxide and carbon nanotube hybrid papers with enhanced electrical and mechanical performance and their synergy in polymer laminates. Int J Mol Sci. 21(22):8585. doi: 10.3390/IJMS21228585.

Wartew GA. 1983. The health hazards of formaldehyde. J Appl Toxicol. 3(3):121–126. doi: 10.1002/JAT.2550030303.

Xiao T, Liu J, Xiong H. 2015. Effects of different functionalization schemes on the interfacial strength of carbon nanotube polyethylene composite. Acta Mech Solida Sin. 28(3):277–284. doi: 10.1016/S0894-9166(15)30014-8.

Xie B, Xu G, Jia Y, Gu L, Wang Q, Mushtaq N, Cheng B, Hu Y. 2021. Engineering carbon nanotubes enhanced hydrophobic membranes with high performance in membrane distillation by spray coating. J Membr Sci. 625: 118978. doi: 10.1016/j.memsci.2020.118978.

Yadav S, Singh Raman AP, Meena H, Goswami AG, Kumar V, Jain P, Kumar G, Sagar M, Rana DK, Bahadur I, Singh P. 2022. An update on graphene oxide: applications and toxicity. ACS Omega. 7(40):35387–35445. doi: 10.1021/ACSOMEGA.2C03171/ASSET/IMAGES/MEDIUM/AO2C03171_0019.GIF.

Yuan YG, Cai HQ, Wang JL, Mesalam A, Reza AMMT, Li L, Chen L, Qian C. 2021. Graphene oxide–silver nanoparticle nanocomposites induce oxidative stress and aberrant methylation in caprine fetal fibroblast cells. Cells. 10(3): 682. doi: 10.3390/CELLS10030682.

Zhang J, Song F, Tao J, Zhang Z, Shi SQ. 2018. Research progress on formaldehyde emission of wood-based panel. Int J Polym Sci. 2018(1):1–8. doi: 10.1155/2018/9349721.

Zheng Q, Xue Q, Yan K, Gao X, Li Q, Hao L. 2008. Effect of chemisorption on the interfacial bonding characteristics of carbon nanotube–polymer composites. Polymer. 49(3):800–808. doi: 10.1016/j.polymer.2007.12.018.

Zhou T, Wang X, Liu X, Xiong D. 2010. Improved thermal conductivity of epoxy composites using a hybrid multiwalled carbon nanotube/micro-SiC filler. Carbon. 48(4): 1171–1176. doi: 10.1016/j.carbon.2009.11.040.